SECOND EUROPEAN CONFERENCE ON EARTHQUAKE ENGINEERING AND SEISMOLOGY, ISTANBUL AUG. 25-29, 2014

EFFECTS OF BOUNDARY REGIONS CONFINEMENT ON THE SEISMIC PERFORMANCE OF FLEXURAL RC STRUCTURAL WALLS

Rafik TALEB[1], Susumu KONO[2], Masanobu SAKASHITA[3] and Masanori TANI[4]

ABSTRACT

In order to study the effects of boundary confined regions on the seismic performance of structural walls, four 40%-scale cantilever type structural walls with or without boundary columns were tested with two levels of the boundary region shear reinforcement. The wall specimens had equal total section area and confined end region area, and equal moment capacity. The moment capacities of structural walls were set at least 1.5 times higher than the shear capacities so that all specimens fail in flexure. The study focused on the effect of boundary columns and confining shear reinforcement on the hysteresis characteristics, such as post-peak backbone curve, ductility, and failure mode. The test results showed that it was efficient to provide boundary columns to reduce damage level and increase deformation capacity. It was also made clear that the axial force level needs to be reduced and the boundary regions be well confined when a structural wall without boundary columns is designed for larger displacement capacity. A finite element (FE) model was built in order to simulate the load-deformation relations as well as cracking and damage patterns of the tested walls. The model is able to simulate the backbone curves with good accuracy. The model is also capable of predicting the ability of boundary columns in reducing damage level.

INTRODUCTION

RC structural walls are frequently used as lateral force-resisting system in building construction because they have sufficient stiffness and strength against damage and collapse. When properly designed, these structural walls can also behave as ductile flexural members. To achieve this goal, the designer should provide adequate strength and deformation capacity. Hence, several experimental and analytical studies were conducted to investigate the behaviour of RC structural walls under lateral loads in order for designers to predict their structural performance when they are subjected to severe seismic excitations (Oh et al., 2006, Zhang et al., 2010,).

In the 2010 Chile Earthquake, a number of structural walls failed in flexure in major cities and raised concerns about the seismic performance of rectangular RC walls. In these earthquakes, severe damage happened to concrete walls in numerous walled buildings leading to partial or total collapse so that structural engineers had to reconsider a false belief that structural walls always behave well. The observed damage patterns at post-earthquake investigations (Figure 1) included crushing of concrete which often spread over more than half of the wall length, fracture under tension or buckling under

[1] Doctoral Student, Tokyo Institute of Technology, Yokohama, Japan, taleb_rafik@yahoo.fr
[2] Professor, Institution, Tokyo Institute of Technology, Yokohama, Japan, kono@serc.titech.ac.jp
[3] Assistant Professor, Kyoto University, Kyoto, Japan, sakashita@archi.kyoto-u.ac.jp
[4] Research Engineer, Building Research Institute, Tsukuba, Japan, mtani@kenken.go.jp

compression of vertical reinforcement at end regions, and global wall buckling (Bonelli et al., 2012). It was reported that lack of adequate confinement and detailing in end regions was one of the main causes of their damages, suggesting that more studies are needed to examine their seismic performance (Wallace et al., 2012). Japanese structural walls normally have boundary columns and beams to provide good confinement to wall panels. In addition to the confining effect, boundary columns carry a large amount of axial force to reduce axial stress level of wall panels leading to less damage conditions. However, the 2010 revised AIJ standard (AIJ, 2010) allows the use of rectangular cross section walls with confined end regions.

Figure 1. Typical RC walls damages at the 2010 Chile earthquake (Wallace et *al.*, 2012)

A research program was undertaken in order to study the effects of end region confinement on the seismic performance of cantilever-type structural walls. Four 40%-scale walls having different cross sectional configurations and transverse reinforcement at the end regions of the walls were constructed and tested under lateral cyclic reversed loading. The test specimens included two specimens with boundary columns and two specimens with rectangular shape section.

TEST SETUP AND EXPERIMENTAL PROCEDURE

Experimental studies were conducted on four 40% scale structural walls designed and constructed by changing the configuration of section (barbell-shape and rectangular sections) and the amount of shear reinforcement in confined regions as shown in Figure. 2. Specimens BC40 and BC80 had confined boundary columns and NC40 and NC80 had no boundary columns but confined boundary regions instead with same thickness as for the wall panel. The wall specimens were tested under lateral cyclic reversal loading in order to evaluate the effects of boundary region size and their confining shear reinforcement on the seismic performance of structural walls.

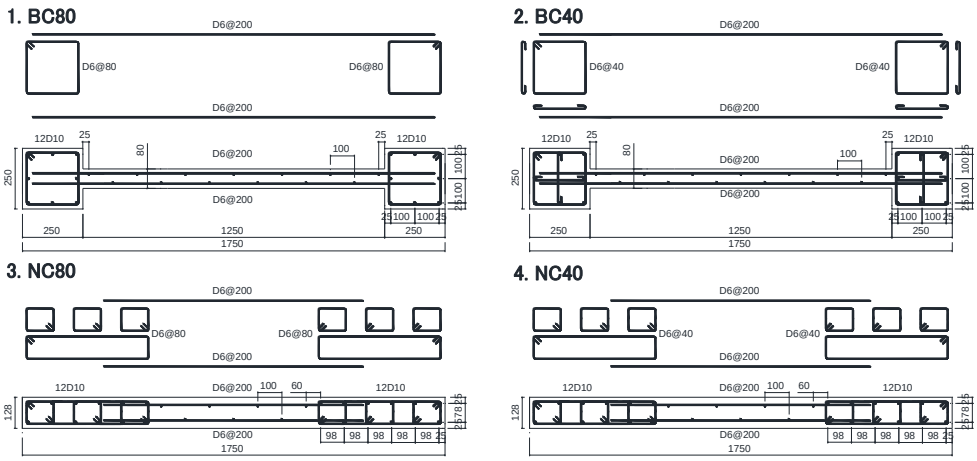

Figure 2. Reinforcement details of the tested wall specimens (unit: mm)

Wall thickness was 128 mm of rectangular wall, while the barbell-shaped wall specimens (BC's specimens) had a wall panel with a thickness of 80 mm and the boundary columns at its both ends with a cross-section of 250 mm×250 mm. The four specimens had same width (1750 mm), nearly same total section area (2250 cm^2 for BC40 and BC 80 and 2240 cm^2 for NC40 and NC80) and also same confined boundary region area (625 cm^2 for BC40 and BC 80 and 666 cm^2 for NC40 and NC80). All specimens were designed to fail in flexure with a shear-to-flexural-capacity ratios were set to more than 1.5. The flexural and shear capacities were calculated based on the AIJ standard (AIJ, 2010). Figure 3 illustrates the vertical reinforcement layouts. Reinforcing bars of D10 were used for longitudinal reinforcement in confined end regions while reinforcing bars of D6 were used for transverse reinforcement and web horizontal and vertical reinforcement. Longitudinal reinforcement at confined region was anchored to an 18 mm thick steel plate placed at the lower stub. Geometrical properties and reinforcement amount are summarized in Table 1.

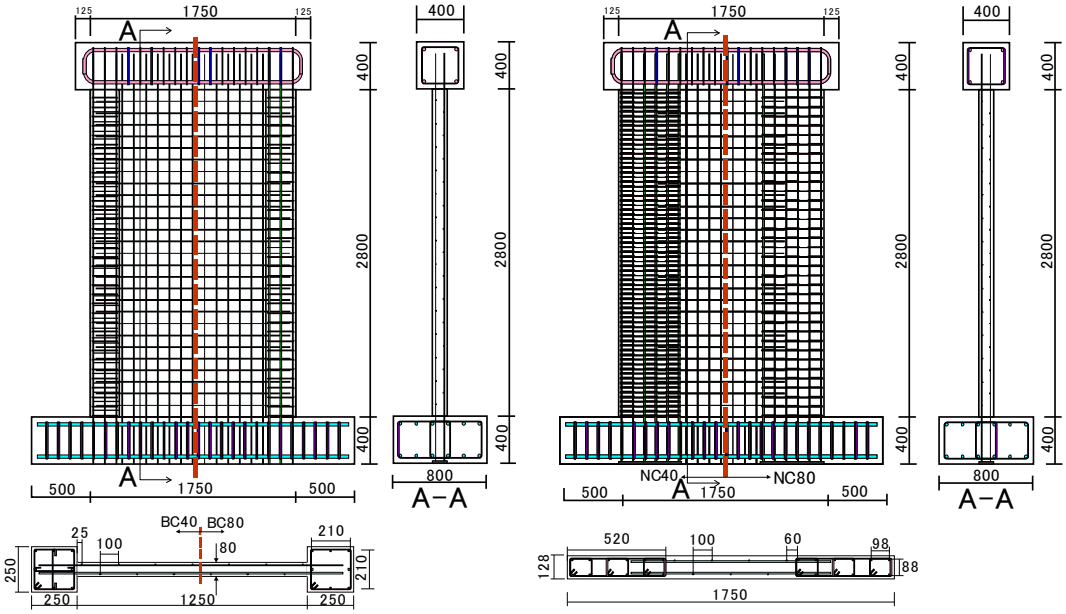

(a) BC40 (left) and BC80 (right) (b) NC40 (left) and NC80 (right)

Figure 3. Dimensions and vertical reinforcement layouts (unit: mm)

Table 1. Specimens geometry and Reinforcement

Specimen	Width & height (mm)	Confined area			Wall panel	
		Section dimension (mm)	Long. Reinf. (rebar ratio)	Shear reinf. (rebar ratio)	Thickness (mm)	Shear reinf. (rebar ratio)
BC80	1750 2800	250x250	8-D10 (0.91%)	2-D6@80 (0.32%)	80	D6@100 Staggered (0.40%)
BC40				3-D6@40 (0.95%)		
NC80		128x520	12-D10 (1.29%)	4-D6@80 (1.24%)	128	D6@100 Staggered (0.25%)
NC40				4-D6@40 (2.47%)		

Ready-mixed concrete with maximum aggregate size of 13mm and slump 18cm was used. Table 2 lists the mechanical properties of concrete and reinforcement. The specimens were casted in two stages, first the foundation beam and second the wall and the loading beam as one part with intentionally roughened surface created at the foundation–wall interface to insure good adherence. The

specimens were tested under reversal quasi-static cyclic loading. Figure 3 shows test setup and loading system. A total axial force of 1500 kN was applied constantly by two hydraulic jacks to keep the axial load level of 0.20 for confined region, corresponding to 0.11 for the total area of the section. Lateral load was applied using a displacement-controlled reverse cyclic load protocol. Each load increment was repeated two times at drift ratios (top horizontal displacement divided by height of lateral load application point) of 0.05%, 0.1%, 0.25%, 0.5%, 0.75%, 1.0%, 1.5%, 2% and 4%.

Table 2. Materials mechanical properties

Specimen	Concrete			Reinf. bar	Steel		
	Compressive strength (MPa)	Young's modulus (GPa)	Splitting strength (MPa)		Yield strength (MPa)	Young's modulus (GPa)	Tensile strength (MPa)
BC80 BC40	59.5	30.9	5.10	D6	387	189	496
NC80 NC40	52.5	30.1	3.66	D10	377	194	533

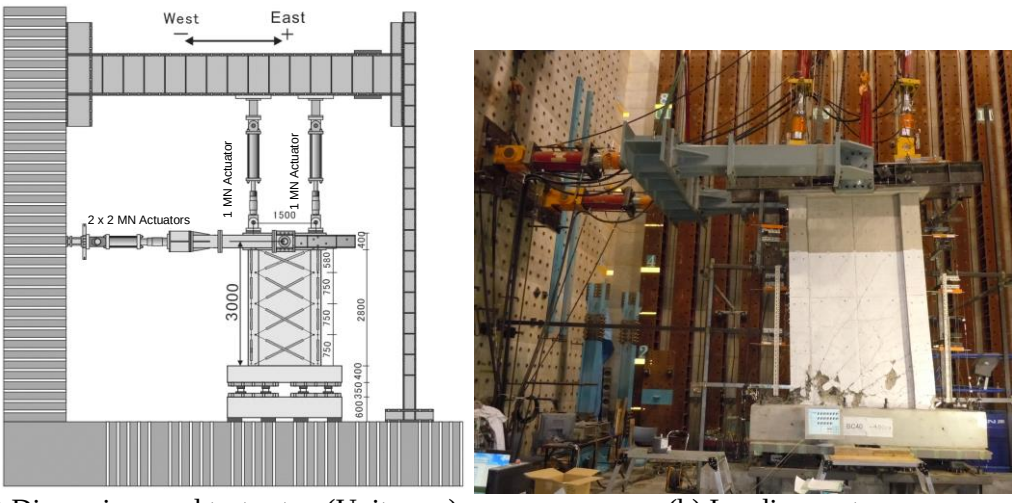

(a) Dimensions and test setup (Unit: mm) (b) Loading system

Figure 3. Test setup and loading system

DAMAGES, HYSTERETIC BEHAVIOR AND FAILURE MODES

Figure 4 shows the experimental lateral load - drift angle relations. The figure shows also the characteristic points: cracking, yielding of longitudinal reinforcement, peak load, and ultimate deformation. All specimens behaved in a flexural manner by yielding of the longitudinal reinforcement, reached the peak point and deformed until failure without significant degradation of lateral load carrying capacity. The longitudinal reinforcement in confined end regions yielded during the cycle of R=±0.1% or ±0.25% for both walls configuration, although the yielding for NC's specimens tended to happen earlier than for BC's specimens. BC40 and BC80 showed no degradation of load carrying capacity until the failure while NC40 and NC80 showed some degradation after reaching peak load due to crushing of core concrete that quickly followed after the peak point. It was remarkable that BC 40 and BC 80 could further sustain load capacity for a larger interval of deformability compared to NC 40 and NC 80. The ultimate failure was caused by crushing of confined concrete and buckling of longitudinal reinforcement of the compression zone. BC40 and BC80 showed no degradation of load carrying capacity until the failure while NC40 and NC80 showed some degradation after reaching peak load due to crushing of core concrete. Small residual drift is probably

due to high concrete strength and axial force which made specimens behave like post-tensioned precast concrete structures.

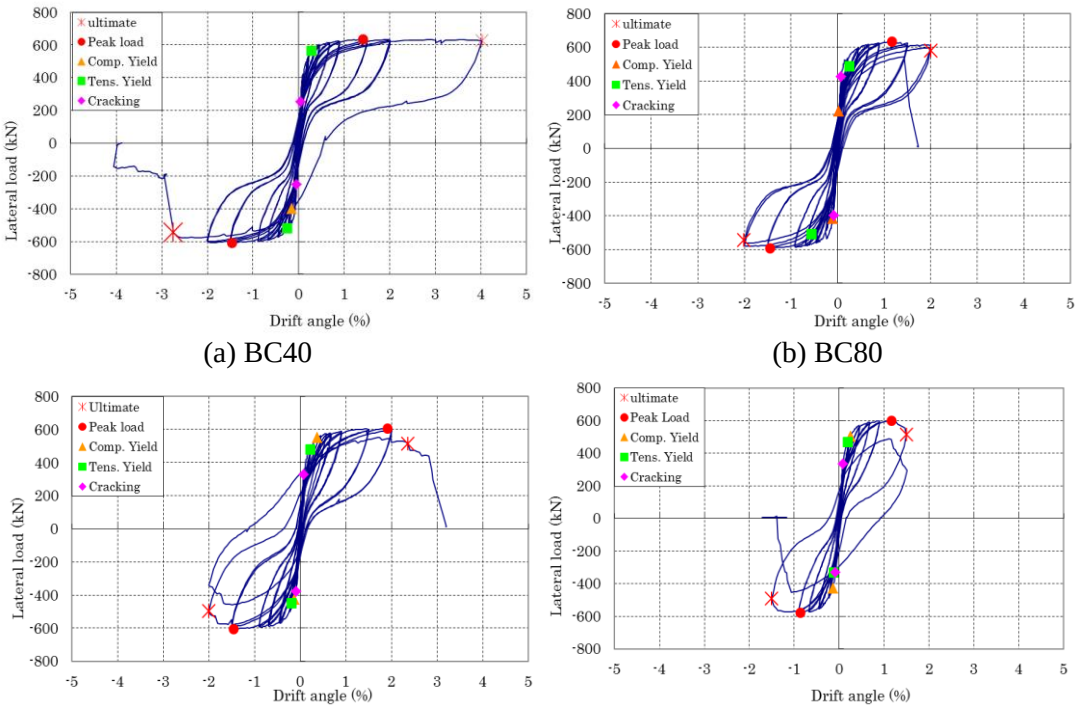

(a) BC40 (b) BC80

(c) NC40 (d) NC80

Figure 4. Experimental lateral load - drift angle relations

Figure 5 shows crack patterns at the final cycle for BC 80, NC 40 and NC 80 specimens and at 2% drift for BC 40. Red and blue lines represent cracks in positive and negative directions, respectively. NC40 and NC80 have flexure-shear cracks which are basically continuous. Although BC40 and BC80 have flexure-shear cracks, flexural cracks and shear cracks are not necessarily continuous at the column interface. On the other hand, it was observed that flexural cracks appeared at small intervals in specimens BC 80 and NC 80 with 80 mm transverse reinforcement spacing compared to specimen BC 40 and NC 40 with 40 mm transverse reinforcement spacing. At the final stage, the failure was brittle because of core concrete crushing. Crushing happened only at the boundary column for BC40 and BC80. However, crushing of concrete extended to the center of the wall panel for NC40 and NC80 and wall panels buckled at the compression region as was seen for the 2010 Chile earthquake. Buckling of longitudinal reinforcement at compression region was observed for all specimens. Figure 6 shows damage patterns at the end of the loading test. Local buckling of concrete crushed region was observed for rectangular walls only.

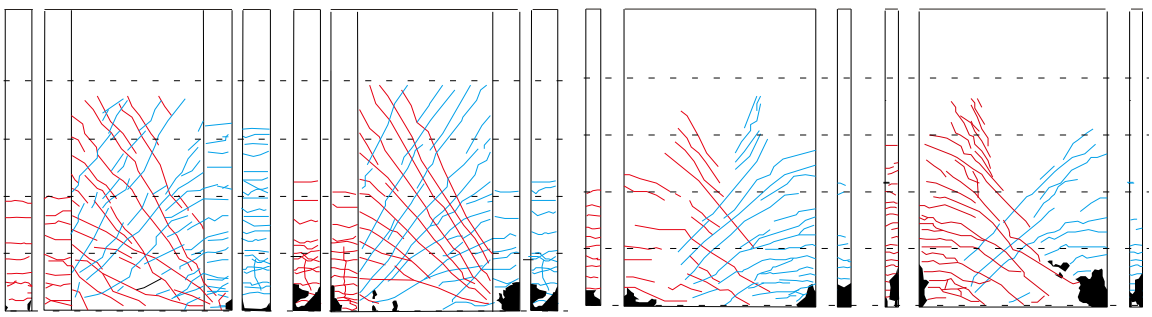

(a) BC40 (-2.0%) (b) BC80 (-2.0%) (c) NC40(-2.0%) (d) NC80 (+1.5%)

Figure 5. Crack patterns at peak load

(a) BC80 (b) NC80

Figure 6. Damage patterns at the end of the loading test for BC 80 and NC80

FLEXURAL AND SHEAR DEFORMATIONS

Displacement transducers for measuring flexural and shear deformations as well as rotation and sliding at wall base were installed. Figure 7 shows the setup of these displacement transducers. Test region was divided vertically into five segment, Z0 region up to 50mm from wall base, three regions Z1, Z2 and Z3 with 750mm height and then Z4 region with 550mm height. Displacement transducers at Z0 were installed to perceive deformation components due to horizontal sliding and vertical pull-out at wall base.

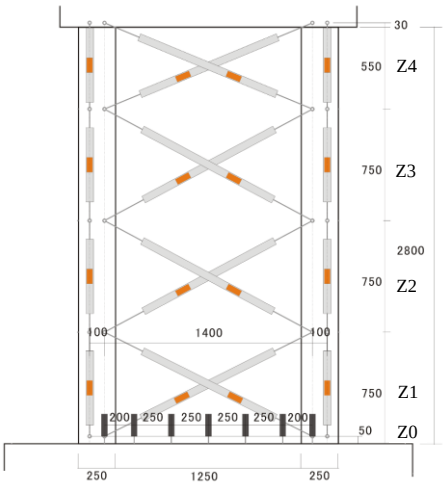

Figure 7. Variation of flexural and shear deformations with top drift angle

The component of flexural, pull-out, shear and sliding of each segment as percentage of total lateral displacement at the peak displacement of the first positive loading cycle of each assigned drift angle is illustrated in Figure 8. The flexural contribution was clearly dominant and constantly as high as 70%. Furthermore, more than 70% of the flexural deformation after yielding concentrated at lower zone (Z1). Similarly, the shear contribution concentrated in the lower part where the longitudinal reinforcement yielded, and remained approximately constant for all peak drift ratio in the inelastic range. Although the shear force in a cantilever wall subjected to a horizontal top load was constant over the height of the wall, the shear deformation was not uniform after concrete cracking and reinforcement yielding.

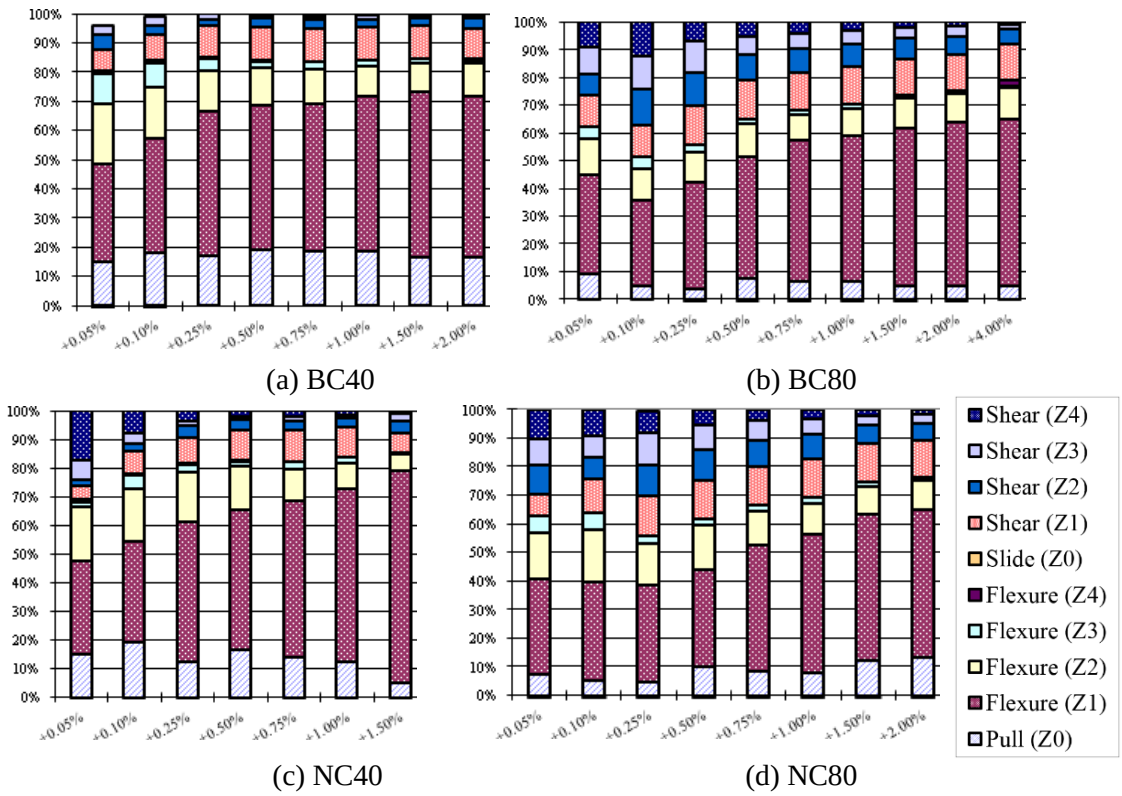

Figure 8. Proportion of deformation components to total deformation

NONLINEAR FINITE ELEMENT ANALYSIS

Numerical analyses were conducted under monotonic loading to investigate the envelope of lateral load response of the tested walls as well as the damage distributions. The analysis was conducted using nonlinear FE program FINAL (ITOCHU, 2010). Figure 9 shows FE mesh for BC's specimens. Four-node plane stress quadrilateral elements were used to model the RC walls. The element size in the wall panel region was about 100 mmx100 mm. The foundation and loading beams were assumed to behave elastically. All nodes at the bottom of the foundation beam were pin-supported to restrain vertical and lateral displacement. The constant axial loads on the top of boundary regions were applied in the first step, and then the lateral load was applied at the loading beam center point under displacement control.

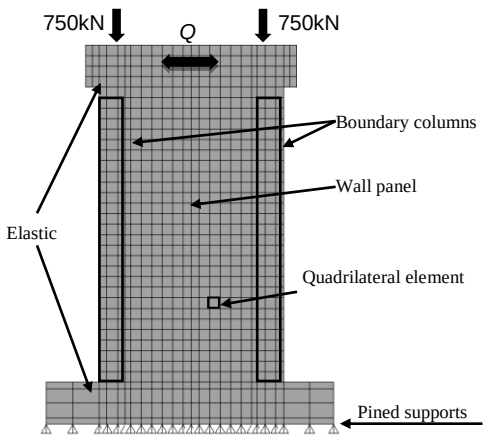

Figure 9. FE mesh for BC 40 and BC 80 specimens

The modified Ahmad model (Naganuma, 1995) for the compressive stress-strain relation of concrete was used for both ascending and descending branchs for unconfined concrete. Mechanical properties of material used in the analysis are thus given in Table 2. For confined concrete at boundary regions, Sakino model (Sakino and Sun, 1994) was used to express stress-strain relation as shown in Figure 10. The Kupfer-Gerstle's failure criterion was adopted for failure in biaxial compression and in tension-compression (Kupfer and Gerstle, 1973). The Naganuma model was adopted for concrete tension stiffing (Naganuma et al., 2004). Uniaxial tensile strength is used for judging cracks under uniaxial and biaxial tension. Stress-strain relationship is assumed to be linear up to cracking. The smeared crack model with a fixed angle concept was used to express cracking of concrete. The shear transfer model after cracking proposed by Naganuma was used (Naganuma, 1991). Smeared reinforcement concept was used for horizontal and transverse reinforcement assuming a perfect bond and truss elements were used to model the vertical reinforcements considering bond effect which was modeled using Elmorsi model (Elmorsi et al., 2000). Stress-strain relation for reinforcement material follows Ciampi's model (Ciampi et al., 1982). All Horizontal and vertical reinforcements were smeared assuming a perfect bond.

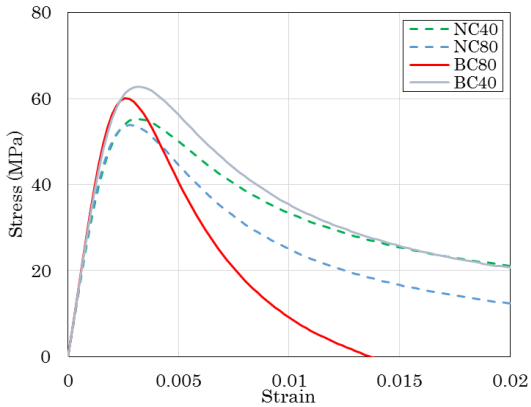

Figure 10. Compressive concrete stress-strain curves for confined end regions

Figure 11 shows lateral load-drift angle relationships obtained analytically and experimentally. Both monotonic and cyclic analytical relations are plotted. Table 3 compare characteristic points: flexural cracking, yielding of longitudinal reinforcement in confined end regions, peak load and ultimate deformation derived from experiment and monotonic analysis. The ultimate deformation is defined by either 20% degradation of load carrying capacity from the peak load or the maximum observed drift. The results show that the model is capable of simulating the entire steps of the nonlinear behavior of the concrete wall such as elastic region, cracking, steel yielding, and peak load with good accuracy. Although the model tends to slightly underestimate ultimate deformation point, the model well capture their trend. The ultimate deformation is defined by either 20% degradation of load carrying capacity from the peak load or the maximum observed drift.

Figure 12 illustrates cracks distribution and damage pattern at ultimate. Crack distribution is less spread in the case of walls with boundary elements compared to that of rectangular walls. Damage for walls with boundary column is concentrated at the outside bottom of boundary columns, while for walls without boundary damage extended along the bottom of confined regions. This is due to the fact that boundary columns carry a large amount of axial force to reduce axial stress level of wall panels to reduce their damage. The built model predicted damage pattern quite well, and has also predicted the ability of boundary columns in reducing damage level and crack distribution.

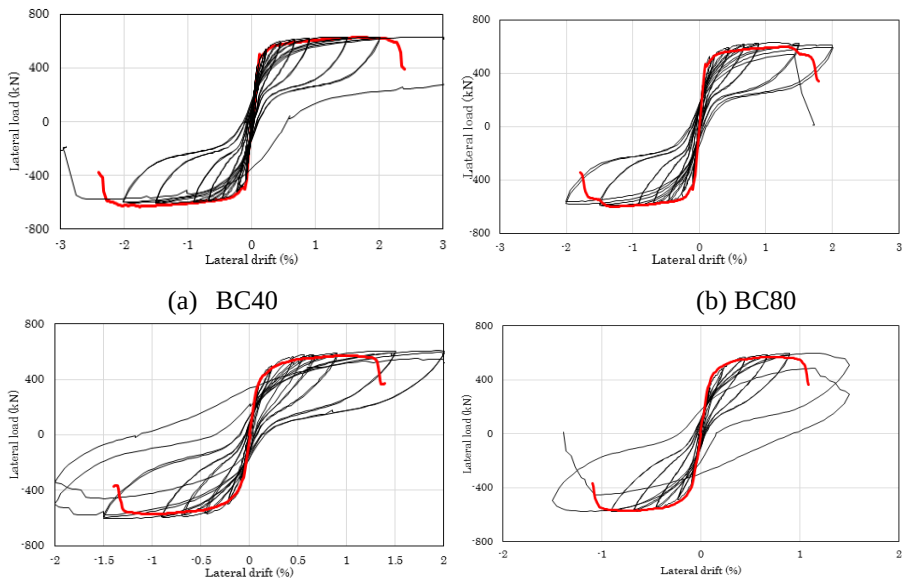

(a) BC40 (b) BC80

(c) NC40 (d) NC80

Figure 11. Experimental and FEM lateral load - drift angle relations

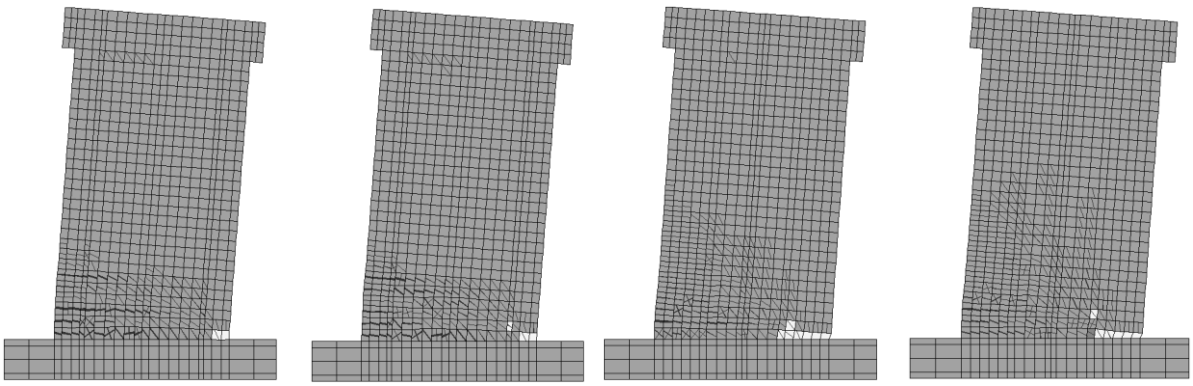

(a) BC40 (b) BC80 (c) NC40 (d) NC80

Figure 12. Damage pattern at ultimate.

Table 3. Materials mechanical properties

Specimen		Cracking		Yielding		Peak		Ultimate	
		Exp.	Num.	Exp.	Num.	Exp.	Num.	Exp.	Num.
BC80	Load (kN)	418/-338	400	487/-507	546	633/-592	599	/	
	Drift (%)	0.08/-0.07	0.07	0.26/-0.33	0.11	1.17/-1.45	1.30	2.00/-2.00	1.72
BC40	Load (kN)	443/-441	346	562/-521	546	634/-608	633	/	
	Drift (%)	0.12/-0.10	0.06	0.29/-0.25	0.11	1.41/-1.47	1.75	4.00/-2.75	2.32
NC40	Load (kN)	334/-331	231	467/-332	505	598/-578	573	/	
	Drift (%)	0.09/-0.08	0.05	0.30/-0.12	0.17	1.16/-0.87	1.07	1.50/-1.50	1.07
NC80	Load (kN)	328/-379	231	478/-449	505	606/-604	571	/	
	Drift (%)	0.07/-0.09	0.05	0.19/-0.20	0.17	1.91/-1.46	0.73	2.38/-2.00	1.33

CONCLUSIONS

Four cantilever type structural wall specimens with or without boundary columns were tested with two levels of the end-region transverse reinforcement to study the effects of end region confinement on their seismic performance. A nonlinear FE analyses was then conducted to simulate load-drift relations and damage progress. The following conclusions can be drawn.

- Walls with boundary columns (barbell-shape section) have larger ultimate drift angle while the transverse reinforcement ratio of columns was less than that of confined region in rectangular walls. However, the final failure mode of barbell-shape section walls was more brittle than that of rectangular section walls. Concrete crushing spread widely over the lower portion with buckling of compression zone for rectangular section walls.
- Flexure deformation is continuously dominant for rectangular section walls while flexural contribution to the total drift increased as walls deformed for barbell-shape section walls.
- The proposed FE model was able to provide accurate backbone curve with important characteristic points such as cracking, yielding, peak and ultimate points. Although the model tends to slightly underestimate ultimate deformation point, the model well capture their trend.
- The built model predicted damage pattern quite well, and has also predicted the ability of boundary columns in reducing damage level and crack distribution

ACKNOWLEDGEMENT

This research work was financially supported by the Ministry of Land, Infrastructure, Transportation and Tourism, Japan.

REFERENCES

[1] Amemiya A and Noguchi H (1990) "Development of Finite Element Analysis Program for High Strength Reinforced Concrete Members (Development of Concrete Model, Part 1)", *Summaries of Technical Papers of Annual Meeting, AIJ*, September, 639-640. (in Japanese)

[2] Architectural Institute of Japan (2010) AIJ Standard for Structural Calculation of Reinforced Concrete Structures, Tokyo, Japan. (in Japanese)

[3] Bonelli P, Restrepo JI, Boroschek R, Carvallo JF (2012) "The 2010 Great Chile Earthquake – Changes to Design Codes". *Proceedings of the International Symposium on Engineering Lessons Learned from the 2011 Great East Japan Earthquake*, Tokyo, Japan, 1-4 March.

[4] Ciampi V, Eligehausen R, Bertero VV, Popov EP (1982) "Analytical model for concrete anchorages of reinforcing bars under generalized excitations", Report No. UCB/EERC82-23, EERC, Berkeley, California.

[5] Elmorsi M., Kianoush MR, Tso WK (2000) "Modeling bond-slip deformations in reinforced concrete beam-column joints", Canadian Journal of Civil Engineering, Vol. 27, 490-505.

[6] ITOCHU Techno-solutions Corportation (2012), FINAL/V11 Help.

[7] Kupfer HB and Gerstle KH (1973) "Behavior of Concrete under Biaxial Stress", *ASCE J. Eng. Mech. Div.*, 99(EM4), 853-866.

[8] Naganuma K (1991) "Nonlinear Analytical Model for Reinforced Concrete Panels under In-Plane Stresses", *Journal of Structural and. Construction Engineering*, Transactions of Architectural Institute of Japan, No.421, 39-48. (in Japanese)

[9] Naganuma K (1995) "Stress-strain Relationship of Concrete under Triaxial Compression", *Journal of Structural and. Construction Engineering*, Transactions of Architectural Institute of Japan, No. 474, 163-170. (in Japanese)

[10] Naganuma K, Yonezawa K, Kurimoto O, Eto H (2004) "Simulation of nonlinear Dynamic response of Reinforced Concrete Scaled Model Using Three-Dimensional Finite Element Method", *Proceedings of the 13th World Conference on Earthquake Engineering*, Vancouver, Canada, 1-6 August, Paper No 586.

[11] Oh YH, Han SW and Choi YW (2006) "Evaluation and Improvement of Deformation Capacities of Shear Walls Using Displacement-Based Seismic Design", *International Journal of Concrete Structures and Materials*, Vol.18, No.1E, 55-61.

[12] Sakino, K. and Sun, Y., (1994). Stress-strain curve of concrete confined by rectilinear hoop, J. Structural and Construction Engineering, Architectural Institute of Japan, No. 461, pp. 95-104. (In Japanese)

[13] Wallace JW, Massone LM, Bonelli P, Dragovich J, Lagos R, Lüders C, Moehle J (2012) "Damage and

Implications for Seismic Design of RC Structural Wall Buildings", *Earthquake Spectra*, 28(S1): S281–S299.

[14] Zhang H, Lu X, Wu X (2010) "Experimental Study and Numerical Simulation of the Reinforced Concrete Walls with Different Stirrup in the Boundary Element", *Journal of Asian Architecture and Building Engineering*, Vol. 9 No.2, 447-454.